Anisotropic tomography of the Atlantic Ocean

Graça Silveira [a,b,*], Eléonore Stutzmann [c]

[a] *Centro de Geofísica da Universidade de Lisboa, Edifício C8, CAMPO GRANDE, P-1749-016 Lisboa, Portugal*
[b] *Instituto Superior de Engenharia de Lisboa, Rua Conselheiro Emídio Navarro, P-1949-014 Lisboa, Portugal*
[c] *Département de Sismologie, Institut de Physique du Globe, 4, Place Jussieu, 75252 Paris Cedex 05, France*

Abstract

We present the first regional three-dimensional model of the Atlantic Ocean with anisotropy. The model, derived from Rayleigh and Love wave phase velocity measurements, is defined from the Moho down to 300 km depth with a lateral resolution of about 500 km and is presented in terms of average isotropic S-wave velocity, azimuthal anisotropy and transverse isotropy.

The cratons beneath North America, Brazil and Africa are clearly associated with fast S-wave velocity anomalies. The mid-Atlantic ridge (MAR) is a shallow structure in the north Atlantic corresponding to a negative velocity anomaly down to about 150 km depth. In contrast, the ridge negative signature is visible in the south Atlantic down to the deepest depth inverted, that is 300 km depth. This difference is probably related to the presence of hot-spots along or close to the ridge axis in the south Atlantic and may indicate a different mechanism for the ridge between the north and south Atlantic. Negative velocity anomalies are clearly associated with hot-spots from the surface down to at least 300 km depth, they are much broader than the supposed size of the hot-spots and seem to be connected along a north–south direction.

Down to 100 km depth, a fast S-wave velocity anomaly is extenting from Africa into the Atlantic Ocean within the zone defined as the Africa superswell area. This result indicates that the hot material rising from below does not reach the surface in this area but may be pushing the lithosphere upward.

In most parts of the Atlantic, the azimuthal anisotropy directions remain stable with increasing depth. Close to the ridge, the fast S-wave velocity direction is roughly parallel to the sea floor spreading direction. The hot-spot anisotropy signature is striking beneath Bermuda, Cape Verde and Fernando Noronha islands where the fast S-wave velocity direction seems to diverge radially from the hot-spots.

The Atlantic average radial anisotropy is similar to that of the PREM model, that is positive down to about 220 km, but with slightly smaller amplitude and null deeper. Cratons have a lower than average radial anisotropy. As for the velocities, there is a difference between north and south Atlantic. Most hot-spots and the south-Atlantic ridge are associated with positive radial anisotropy perturbation whereas the north-Atlantic ridge corresponds to negative radial anisotropy perturbation.

1. Introduction

The Atlantic Ocean occupies an elongated S-shaped basin extending in a north–south direction. It is the second largest ocean and has a relatively small number of islands. The most striking feature of the ocean

* Corresponding author. Tel.: +351-217-500-812;
fax:+ 351-217-500-977.
E-mail address: gracams@correio.cc.fc.ul.pt (G. Silveira).

bottom topography is a great submarine mountain range, the mid-Atlantic ridge (MAR) which separates the ocean into two large troughs with depths averaging between 4 and 6 km. Transverse ridges running between the MAR and continents divide the ocean floor into numerous basins.

The mid-Atlantic ridge axis is roughly north–south in the south Atlantic and deviates to the west in the north Atlantic. On the other hand, hot-spots are all aligned along a roughly north–south direction. They are located along the ridge in the south Atlantic and of the ridge in the north Atlantic. Understanding the role of hot-spots in the Atlantic opening is important from a geodynamic point of view because hot-spots and ridges are the two main forms of up-welling at the interior of the Earth.

Four cycles of closing and re-opening of paleo-ocean basins, the Wilson cycle (e.g. Windley, 1984), have been reported for the Atlantic, each of them lasting 400–500 My (Anderson, 1982; Goodwin, 1985; Hoffman, 1989). The last re-opening of the Atlantic Ocean started 180 My ago at the Mexico Gulf and the young mid-Atlantic ridge started to migrate southward and northward. The south end of the south Atlantic opening started 130 My ago and migrated toward the Equator. The central and south Atlantic openings met around 120 My ago in the Equatorial Atlantic. Finally, the north Atlantic started opening 113 My ago, progressively dissociating Greenland from North America and from Eurasia. Since 33 My, the morphology of the Atlantic has remained stable and the current mid-Atlantic ridge spreading rate is very small, varying between 1 and 4 cm per year.

For understanding the driving mechanisms of the opening of the Atlantic, the depth extent of ridge and hot-spots is an important constraint. Seismic data provide unique information above the hot-spots and ridge seismic signature via three-dimensional tomographic images of the mantle. Global tomographic models enable us to distinguish only the mid-Atlantic ridge (e.g. Li and Romanowicz, 1996; Mégnin and Romanowicz, 2000). Information about smaller scale structures of the Atlantic can only come from regional studies. The first regional three-dimensional model of the Atlantic was proposed by Honda and Tanimoto (1987) using a waveform inversion technique. Later, Mocquet and Romanowicz (1990) inverted surface wave phase velocities and Grand (1994)

inverted S-wave travel times to obtain new three-dimensional models of the Atlantic. The robust feature of these models is the mid-Atlantic ridge which is characterized by a low velocity anomaly down to about 200 km.

In order to better constrain the seismic structure of the Atlantic, we have constructed the first anisotropic three-dimensional model of the Atlantic Ocean. The S-wave seismic velocity model is derived from Rayleigh and Love wave phase velocity measurements. The Rayleigh wave phase velocities were first presented by Silveira et al. (1998). We computed our S-wave velocity model down to 300 km depth with a lateral resolution of about 500 km. Hot-spots and the ridge are associated with low velocity anomalies. We discuss their depth extent and connections in the framework of mantle convection.

2. Method

We computed fundamental mode surface wave phase velocities for many epicenter-to-station paths by cross-correlating data with normal mode synthetic seismograms using the PREM model (Dziewonski and Anderson, 1981) as a reference. The influence of crustal structure on surface waves is very important at short periods and decreases with increasing periods (e.g. Stutzmann and Montagner, 1994). It can bias deep structure recovery, though the frequency content of our dataset is dominantly long period, ranging from 55 to 250 s. Therefore, phase velocity crustal perturbations were computed for the 3SMAC model (Nataf and Ricard, 1996) and subtracted from our dataset.

In a first step, phase velocities obtained path by path were inverted to obtain their anisotropic lateral variations. According to Smith and Dahlen (1973) for a slight anisotropic earth, the local phase velocity C at a given point M, can be expressed, for each angular frequency ω,

$$
\begin{aligned}
C(\omega, M, \psi) = C_0(\omega, M)[1 &+ \alpha_1(\omega, M)\cos(2\psi) \\
&+ \alpha_2(\omega, M)\sin(2\psi) + \alpha_3(\omega, M) \\
&\times \cos(4\psi) + \alpha_4(\omega, M)\sin(4\psi)] \quad (1)
\end{aligned}
$$

where ψ is the azimuth, C_0 the azimuthal average phase velocity (called hereafter isotropic phase velocity) and α_i are the phase velocity azimuthal anisotropy

coefficients. Using this phase velocity expansion, Montagner and Nataf (1986) have developed a regionalization method which has been used separately for Rayleigh and Love waves. The Rayleigh wave phase velocity maps are presented in a first paper by Silveira et al. (1998) together with the method and the resolution tests.

Montagner and Nataf (1986) demonstrated that Rayleigh wave phase velocity is mainly sensitive to azimuthal anisotropy via the 2ψ-coefficients (α_1 and α_2) of Eq. (1) and Love wave phase velocity via the 4ψ-coefficients (α_3 and α_4). Therefore, we inverted versus depth Rayleigh and Love wave local phase velocities parameterized using three parameters each: C_{0_R}, α_{1_R} and α_{2_R} for Rayleigh waves and C_{0_L}, α_{3_L} and α_{4_L} for Love waves.

Montagner and Nataf (1986) proposed to describe the Earth by an orthotrope model, that is a transverse isotropic medium with a symmetry axis in any direction. If the mantle olivine is oriented along the maximum flux direction, then the symmetry axis gives the direction of maximum flux. In an orthotrope model, the elastic tensor can be described by 13 parameters, A, C, F, L, N, B_c, B_s, H_c, H_s, G_c, G_s, E_c, E_s. The first five parameters (A, C, F, L, N) describe the equivalent transverse isotropic medium with vertical symmetry axis. They correspond to the isotropic term, C_0, of Eq.(1) and the discrepancy between Love and Rayleigh phase velocities. The parameters $B_{s,c}$, $G_{s,c}$, $H_{s,c}$ describe the 2ψ azimuthal variations whereas the parameters $E_{s,c}$ define the 4ψ variations. Starting from the partial derivative of a transverse isotropic medium with vertical symmetry axis, it is then simple to compute phase velocity partial derivatives with respect to an anisotropic medium having a symmetry axis in any direction. We have the following relations (e.g. (Montagner, 1986; Lévêque et al., 1989)) for Rayleigh wave phase velocity perturbation, δC_R:

$$
\begin{aligned}
\delta C_R = {} & \frac{\partial C_R}{\partial A}(\delta A + B_c \cos 2\psi + B_s \sin 2\psi + E_c \cos 4\psi \\
& + E_s \sin 4\psi) + \frac{\partial C_R}{\partial C}\delta C + \frac{\partial C_R}{\partial F}(\delta F + H_c \cos 2\psi \\
& + H_s \sin 2\psi) + \frac{\partial C_R}{\partial L}(\delta L + G_c \cos 2\psi \\
& + G_s \sin 2\psi)
\end{aligned} \tag{2}
$$

Similarly for Love wave phase velocity perturbations, δC_L, we have:

$$
\begin{aligned}
\delta C_L = {} & \frac{\partial C_L}{\partial L}(\delta L - G_c \cos 2\psi - G_s \sin 2\psi) \\
& + \frac{\partial C_L}{\partial N}(\delta N - E_c \cos 4\psi - E_s \sin 4\psi)
\end{aligned} \tag{3}
$$

The inversion is performed using the 13 parameters per layer but the dataset cannot resolve all the parameters. It has been shown that Rayleigh waves are mainly sensitive to parameters L, G_c and G_s and Love waves are mainly sensitive to parameters N, E_c and E_s (Montagner and Nataf, 1986). Then, the three-dimensional model can be described by the following parameters for a given depth:

$$
V_{SV} = \sqrt{\frac{L + G_c \cos 2\psi + G_s \sin 2\psi}{\rho}} \tag{4}
$$

$$
\xi = \frac{N - E_c \cos 4\psi - E_s \sin 4\psi}{L + G_c \sin 2\psi + G_s \sin 2\psi} = \left(\frac{V_{SH}}{V_{SV}}\right)^2 \tag{5}
$$

where V_{SV} is the SV-wave velocity and V_{SH} the SH-wave velocity. Love wave azimuthal coverage is less uniform than that of Rayleigh waves and so the parameters E_c and E_s cannot be correctly retrieved. Therefore, we will not consider azimuthal variation of ξ parameter which becomes $\xi \simeq N/L$.

The three-dimensional model can be obtained either by first inverting each path phase velocity versus depth and then determining the lateral variations of the model or by inverting versus depth the phase velocity lateral variations. This second procedure is preferred because the inversion for retrieving phase velocity lateral variations is linear whereas the relationship between phase velocities and depth dependent velocity model is not.

The anisotropic three-dimensional model is computed using an iterative inverse algorithm (Tarantola and Valette, 1982) which takes into account the phase velocity error maps as a priori errors. Depth is discretized per layer and a Gaussian correlation is introduced between adjacent depths. Resolution tests are presented in the appendix.

The tomographic model presented in this paper is described in terms of isotropic SV-wave velocity defined by $V_{SV} = \sqrt{L/\rho}$, azimuthal anisotropy which is represented by an horizontal vector defined by G_c and

G_s and radial anisotropy which corresponds to $\xi - 1$ parameter.

3. Data

The dataset consists of long period (LH) seismograms recorded by GEOSCOPE and IRIS stations in and around the Atlantic Ocean for events of magnitude 5.8–7. In total, 1300 Rayleigh wave phase velocities and 600 Love wave phase velocities were computed. The dataset is limited because the Atlantic Ocean is characterized mostly by earthquakes of magnitude smaller that 5.8 for which no CMT is computed. Furthermore, there is an evident lack of broadband stations in and around the ocean. Fig. 1 displays the data coverage. Rayleigh wave phase velocity lateral variations and errors are presented in the paper by Silveira et al. (1998). Love wave phase velocity maps have been determined using the same technique. Fig. 2 presents the phase velocity maps for both Rayleigh and Love waves at a period of 88 s. Parameters used in this inversion and tests on the inversion reliability can be found in the paper by Silveira et al. (1998). In Appendix A is also presented a synthetic test showing that phase velocity and anisotropy are correctly recovered with the path coverage of Fig. 1 in the area corresponding to the maximum path coverage. In Appendix B is presented a test on the phase velocity inversion versus depth.

The anisotropic three-dimensional S-wave velocity model derived from these datasets is presented in the next sections.
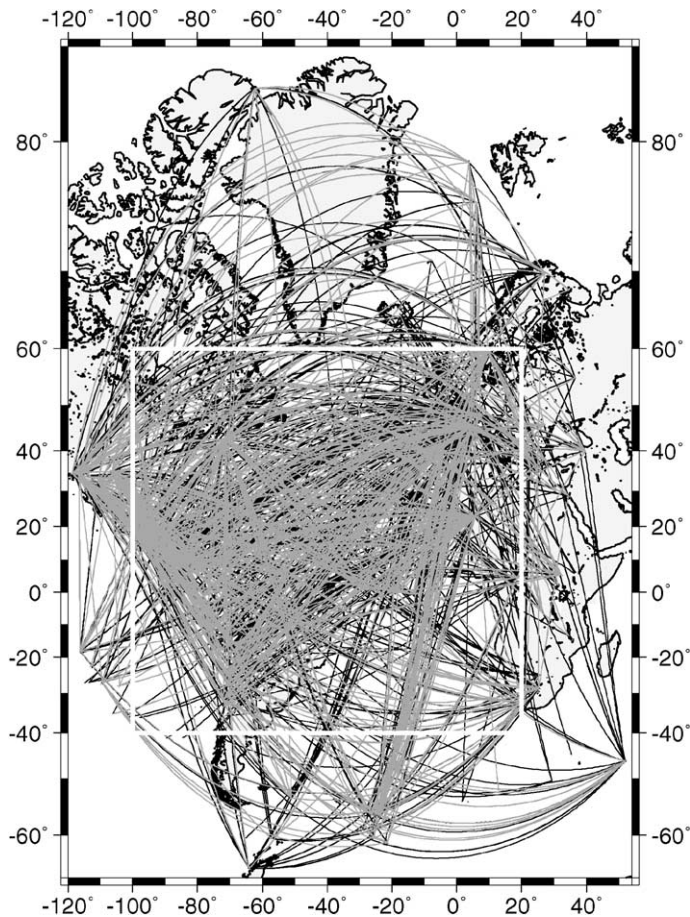

Fig. 1. Geographical paths between epicenters and stations for Rayleigh waves (solid black line) and Love waves (dashed grey line).
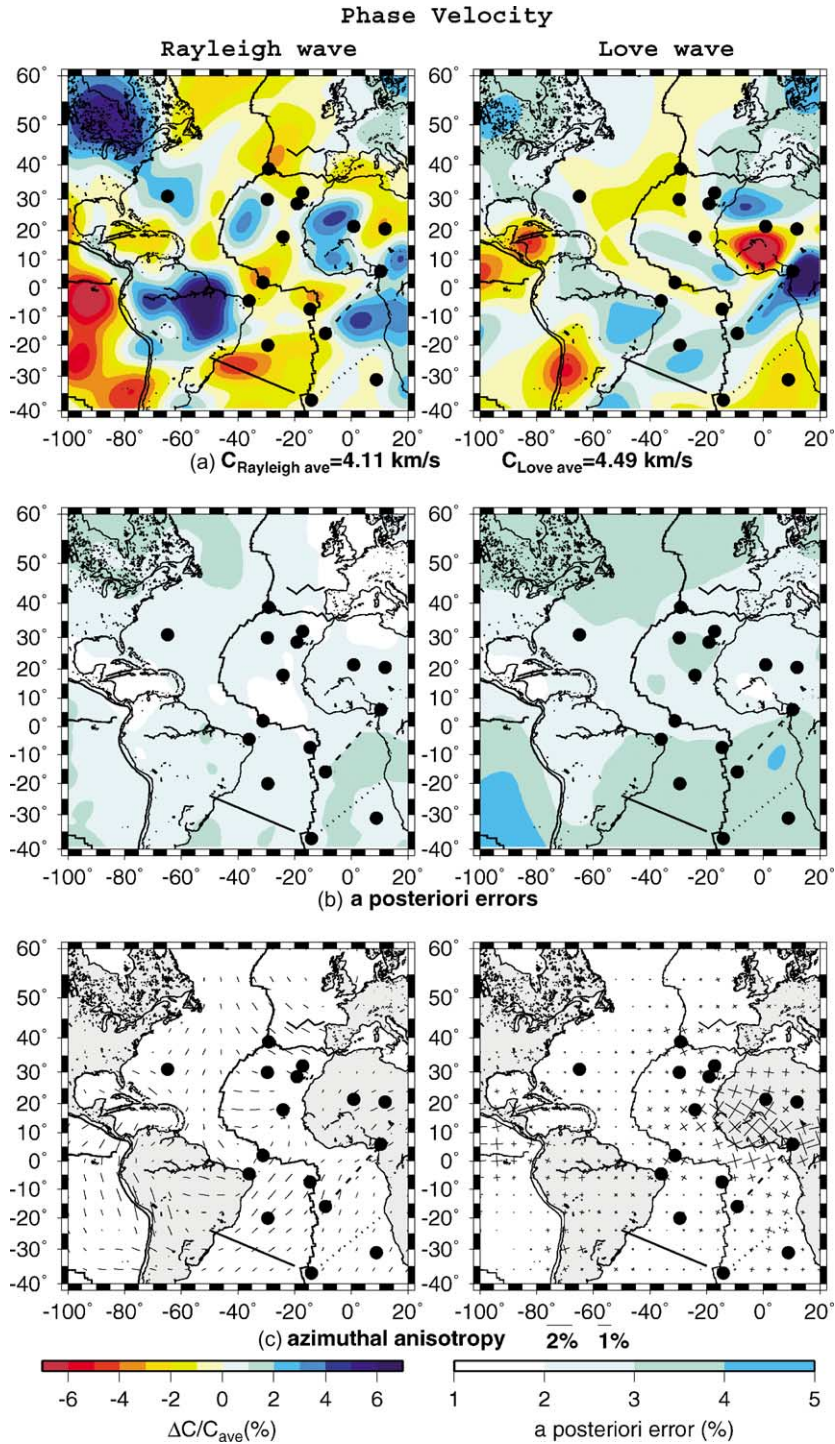
Fig. 2. Phase velocity maps at a period of 80 s for Rayleigh waves (left) and Love waves (right). From top to bottom: phase velocity lateral variations, phase velocity errors, and anisotropy.
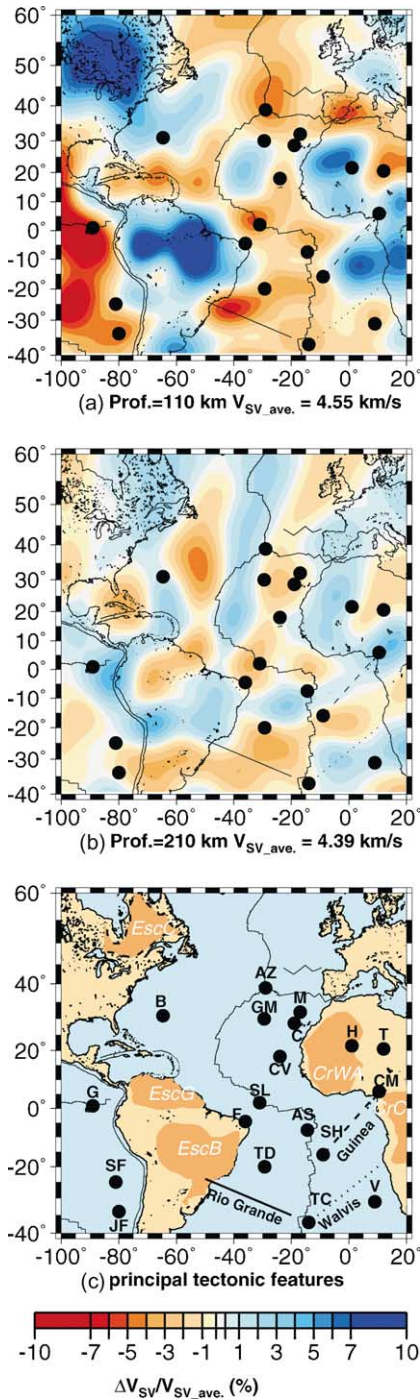
Fig. 3. S-wave velocity lateral variations with respect to the average value written at the bottom on each plot for depths: (a) 110 km; and (b) 210 km depth; (c) plate boundaries, hot spot locations and some geological features-after Crough (1983).

4. Atlantic tomographic model

Atlantic hot-spots are all aligned along a roughly north–south direction along the ridge axis in the south Atlantic and off the ridge axis in the north Atlantic (see Fig. 3c for a compilation of Crough (1983), Melson and O'Hearn (1986), Aslanian (1993)) Hot-spots are clearly associated with negative S-wave velocity anomalies in our tomographic maps (Fig. 3a and b). These anomalies have a large amplitude from the surface down to about 200 km. The amplitude decreases at greater depths but hot-spots remain visible down to the deepest depth inverted. The hot-spot velocity anomalies are much broader that the supposed size of the hot-spots and seem to be connected along a north–south direction from the surface down to at least 300 km depth (Figs. 3 and 4). Indeed, the Azores hot-spot deviates from the ridge axis at depth toward the south in the direction of the Capo Verde hot-spot (Fig. 4a).

The mid-Atlantic ridge is caraterized by a negative velocity signature between 100 and 150 km depth (Fig. 3a). Closer to the surface, The ridge is also slow everywhere except in the part of the ridge having the slowest opening rate, that is between 20 and 30°N, where we observe a small shallow positive anomaly (Fig. 4b). Deeper than 150 km, there is a striking difference between the northern and southern ridge structure (Fig. 4b). At the north (60–10°N), the ridge is only associated with low velocity at shallow depth (down to 150–200 km). On the contrary, in the south (10–60°S) the ridge low velocity anomaly is observed down to the deepest depth inverted, 300 km. The main difference between the northern and southern Atlantic is the presence of hot-spots along or close to the ridge axis in the south. Therefore, the northern part of the ridge

Melson and O'Hearn (1986), Aslanian (1993). **CSh**, Canadian Shield; **GSh**, Guyana Shield; **BSh**, Brazilian Shield; **WAc**, West African craton; **Cc**, Congo craton. Circles designate hot-spots, from top to bottom: **AZ**, Azores; **M**, Madeira; **B**, Bermuda; **GM**, Great Meteor; **H**, Hoggar; **T**, Tibesti; **C**, Canaries; **CV**, Cape Verde; **CM**, Cameroon; **SL**, Sierra Leone (Shilling et al. (1994)); **G**, Galapagos; **F**, Fernando de Noronha; **AS**, Ascension; **SH**, Santa Helena; **TD**, Trindade; **SF**, San Felix; **V**, Vema; **TC**, Tristan da Cunha; **JF**, Juan Fernandez. Lines correspond to hot-spot traces.
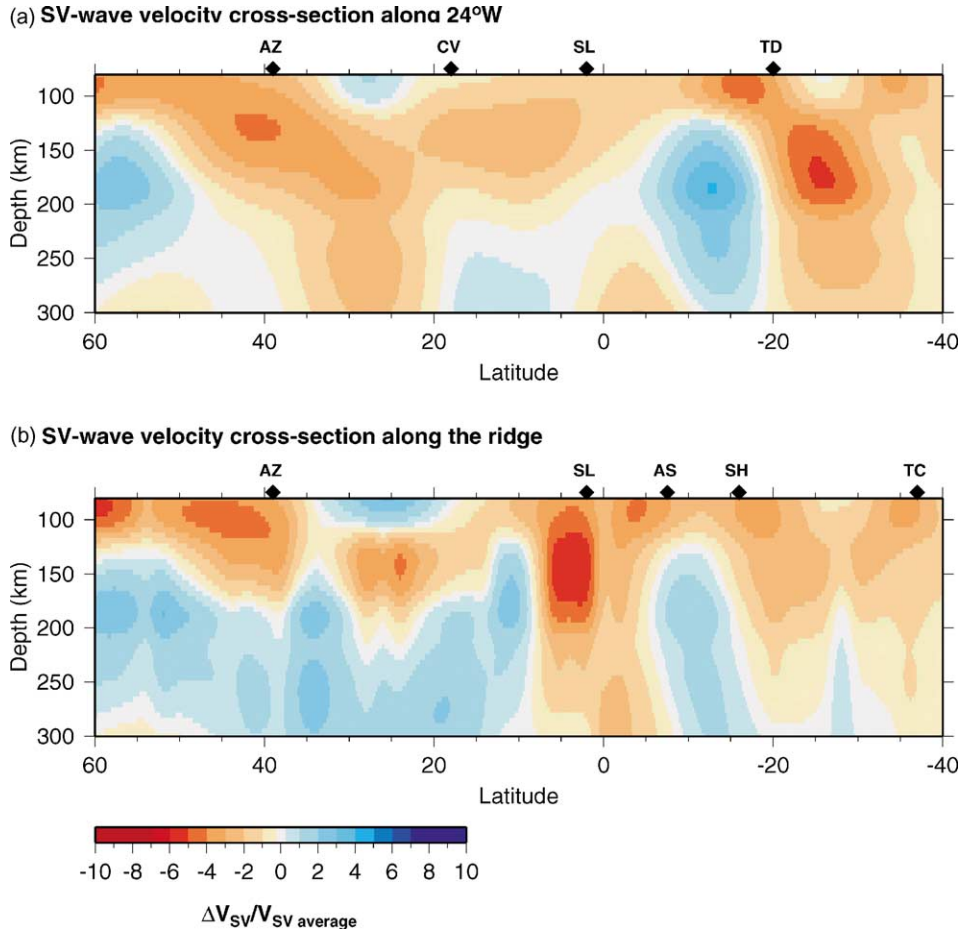
Fig. 4. Map of the Atlantic Ocean with the cross-section locations. Cross-section of the S-wave velocity perturbation: (a) along the longitude 24°W passing through the Azores; (b) along the mid-Atlantic ridge.

probably correspond to a shallow and passive feeding caused by the plate separations, while the southern part of the ridge is fed by a deeper source which also feeds the hot-spots.

At 110 km depth, a fast anomaly is extenting from Africa into the Atlantic Ocean at 10°E 10°S between the Guinea rise and the Walvis rise. It is located in the zone defined by McNutt (1998) as the Africa superswell area. Several models suggest that the superplume is rising from the core-mantle boundary (e.g. Ritsema et al., 1999). Our model shows that the hot material rising from below does not reach the surface in this area but may be pushing the lithosphere upward.

The cratons beneath North America, Brazil and Africa are clearly associated with fast S-wave velocity anomalies. In Africa, the two fastest anomalies are located beneath West African and Gabon cratons separated by an intermediate zone which is in line with the Saint Helena hot-spot track. The amplitude of the craton positive anomaly is large down to about 200 km. Deeper, the anomaly amplitude decreases and the root of these cratons is probably around 250 km depth.

4.1. S-wave azimuthal anisotropy

The S-wave azimuthal anisotropy presented in Fig. 5 is quite similar to the Rayleigh wave phase

AZIMUTHAL ANISOTROPY: $\overline{2\%}$ $\overline{1\%}$

(a) **Depth=110 km**

(b) **Depth=210 km**

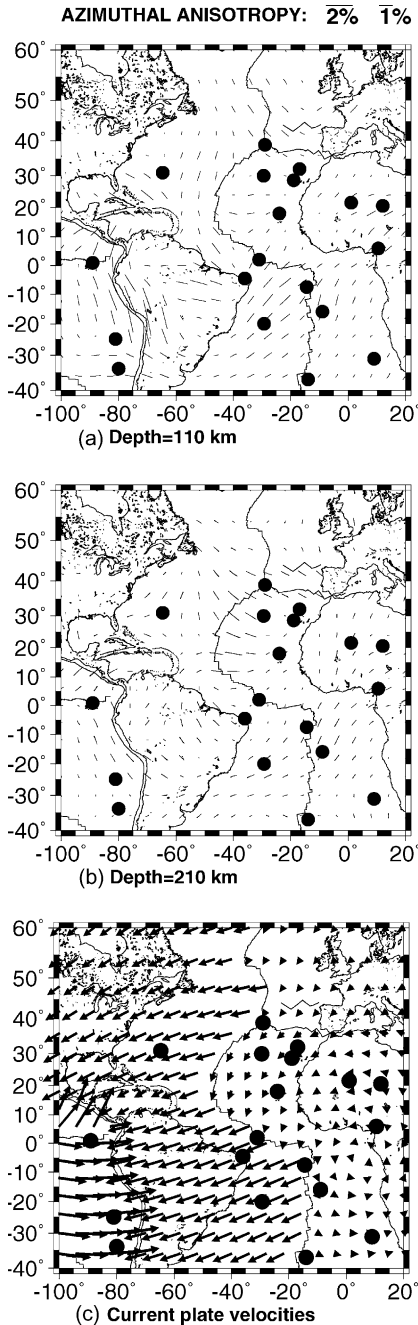
(c) **Current plate velocities**

Fig. 5. S-wave velocity azimuthal anisotropy for (a) 110 km; (b) 210 km depth. The S-wave velocity fast directions are given by the bars azimuth. The length of the bars are proportional to the intensity with respect to the scale on top of the figure. (c) Current plate velocities calculated from model NUVEL-1 (Gripp and Gordon, 1990).

velocity anisotropy pattern obtained in a previous paper (Silveira et al., 1998) because S-wave azimuthal anisotropy is mainly sensitive to Rayleigh wave phase velocity. The resolution of anisotropy direction is best when the path azimuthal coverage is uniform which is the case in this study except at the edges of the studied area (Pacific Ocean, North America and Europe) where most of the path have the same directions and therefore bias the anisotropy results.

As for velocities, the anisotropy pattern is different in the north and south Atlantic (Fig. 5). At 110 km depth, south Atlantic anisotropy directions are consistent with current plate velocities relative to hot-spots calculated from the model NUVEL-1 (Gripp and Gordon, 1990) (Fig. 5c). These directions remain stable with increasing depth. At the Ascension Island (100 km west of the MAR), our anisotropy direction is consistent with body wave anisotropy measurement obtained by Wolfe and Silver (1998) using SS-wave splitting.

In the north Atlantic, the anisotropy directions remain stable with increasing depth except near the ridge between 20 and 30°N, in the region characterized by the shallow positive S-wave velocity anomaly. In this region, the anisotropy is weak at shallow depth and rotate to become perpendicular to the ridge axis at 150 km depth and deeper.

The western part of the north Atlantic Ocean shows a roughly north–south fast direction which is parallel neither to present-day plate motion (Fig. 5c) nor to a simple model of flow diverging horizontally from the ridge. This north–south orientation agrees with the anisotropy direction obtained by Kuo et al. (1987) from shear waves.

Hot-spot anisotropy signature is striking beneath Bermuda, Cape Verde and Fernando Noronha islands where the fast S-wave velocity direction seems to diverge radially from the hot-spots.

Beneath continents, we observe a rotation of the S-wave fast axis with depth. This effect is clear beneath shields like the Brazilian, Guyana and West African Craton. Close to the surface the fast S-wave velocity direction is nearly parallel to present absolute plate motion. As the depth increases, the azimuthal anisotropy amplitude decreases and the directions become almost perpendicular to the present absolute plate motion.
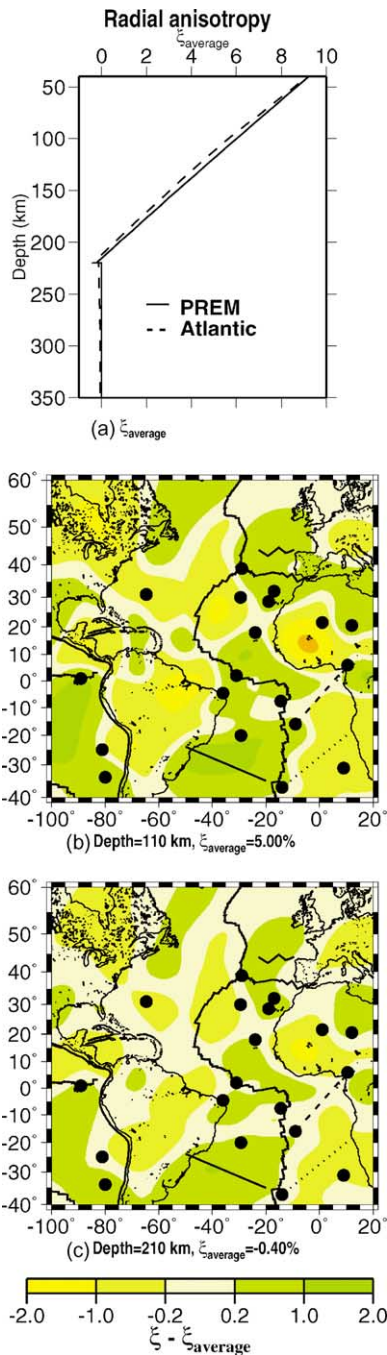
Fig. 6. (a) Average S-wave velocity radial anisotropy, ξ, as a function of depth for the Atlantic area (dashed line) and the PREM model (solid line). (b, c) Radial anisotropy lateral variation with respect to the average value written at the bottom of each plot and for 110 and 210 km depth, respectively.

4.2. Radial anisotropy

The average S-wave velocity radial anisotropy as a function of depth is very similar to that of the PREM model but sligtly shifted toward more negative amplitudes (Fig. 6). It is positive down to about 220 km depth and becomes nul deeper. To a first order approximation $\xi - 1 \simeq 2 \times (V_{SH} - V_{SV})/V_{SV}$. Therefore, the positive radial anisotropy observed down to 220 km depth means that SH-wave velocity is larger than SV-wave velocity and the flow is dominantly horizontal in the area. Deeper, no significant anisotropy is observed.

The average radial anisotropy presented on Fig. 6a is used as reference model for plotting radial anisotropy lateral variations as a function of depth on Fig. 6b and c. The anisotropy amplitude decreases with increasing depth but its pattern remain stable. In the south, the ridge and the Rio Grande Rise are associated with higher than average anisotropy, whereas in the north between 20 and 35°N the anisotropy is lower than average, but its absolute value remains positive. These results are in agrement with the interpretation of the SV-wave velocity maps. The radial anisotropy indicates a rather horizontal flow in the north Atlantic where the mid-Atlantic ridge is a shallow seismic structure that may correspond to a passive feeding caused by plates separation. On the other hand, the radial anisotropy indicates a rather vertical flow in the south Atlantic where the mid-Atlantic ridge seismic signature is deeper, indicating a deeper source.

Fig. 6 also shows that the cratons of Brazil, Guyana and West Africa are all associated with lower than average radial anisotropy at both 110 and 210 km depth indicating a dominantly horizontal flow. This result is consistent with stable and old tectonic features such as cratons.

5. Conclusions

Rayleigh and Love wave phase velocities computed path by path have enabled us to determine the first regional three-dimensional model of the Atlantic Ocean that takes into account anisotropy. The model is defined from the Moho down to 300 km depth with a lateral resolution of about 500 km and it is presented in terms of average isotropic

S-wave velocity, azimuthal anisotropy and transverse isotropy.

The cratons beneath North America, Brazil and Africa are clearly associated with fast S-wave velocity anomalies and negative radial anisotropy perturbations. The mid-Atlantic ridge is a shallow structure in the north Atlantic corresponding to a negative velocity anomaly down to about 150 km depth and a negative radial anisotropy perturbation. In contrast, in the south Atlantic, the ridge negative signature is visible down to the deepest depth inverted (300 km) and the radial anisotropy perturbation is positive. This difference is probably related to the presence of hot-spot at or near to the south-Atlantic ridge axis. Hot-spots correspond to negative velocity anomalies from the surface down to at least 300 km depth which are much broader than the supposed size of the hot-spots and which seem to be connected along a north–south direction in the entire upper mantle. Therefore, the northern part of the ridge probably correspond to a shallow and passive feeding caused by the plate separation. On the contrary, the southern part of the ridge and hot-spot is fed by a deeper source which also feeds hot-spots.

At 110 km depth, a fast S-wave velocity anomaly is extenting from Africa into the Atlantic Ocean within the zone defined as the Africa superswell area. This result indicates that the hot material rising from below does not reach the surface in this area but may be pushing the lithosphere upward.

In most of the Atlantic, the azimuthal anisotropy directions remain stable with increasing depth. Close to the ridge, the fast S-wave velocity direction is roughly parallel to the sea floor spreading direction. The western part of the north Atlantic Ocean shows a roughly north–south fast direction consistent with body waves measurements. Hot-spot anisotropy signature is striking beneath Bermuda, Cape Verde and Fernando Noronha islands where fast S-wave velocity direction seems to diverge radially from the hot-spots.

The Atlantic radial anisotropy pattern is similar to that of the PREM model but slightly shifted toward weaker amplitudes. It is positive down to about 220 km depth and becomes null deeper. The radial anisotropy perturbations are consistent with the interpretation of the SV-wave velocity maps. Cratons associated with rather horizontal flows. The mid-Atlantic ridge corresponds rather horizontal flows in the north Atlantic and rather vertical flows in the south Atlantic.

Appendix A. Tests on the phase velocity lateral variation inversion

Tests and parameters of the regionalization method are extensively discussed in a previous paper by Silveira et al. (1998). Hereafter, we present a synthetic experiment to demonstrate the reliability of the phase velocity lateral variation and anisotropy maps. The path coverage of Fig. 1 corresponding to the real dataset is used. The anisotropic phase velocity model is presented on Fig. 7a and b. It has be chosen to reproduce the main features obtained by the inversion of the real datset. We consider several positive and negative anomalies of ±5% with respect to the reference model and anisotropy anomalies of 2% in different directions. The inversion is performed using the same parameters (a priori error, correlation length) as for the real data. The inversion results presented on Fig. 7c and d shows that the phase velocity anomalies are correctly recovered both in location and amplitude though the anomalies are smoothed by the correlation length of 500 km used in the inversion. Fig. 7b and c show that the large anisotropy anomalies are correctly recovered in the areas where the path azimuthal coverage is uniform and that the azimuthal anisotropy results should not be interpreted at the edges of the area of interest.

Appendix B. Tests on the inversion versus depth

This appendix presents tests on the phase velocity inversion for retrieving the SV-wave velocity and radial anisotropy as a function of depth.

We considered a model perturbation located between 100 and 220 km depth which respect the PREM model. We introduced a 5% SH-wave velocity perturbation and a 3% SV-wave velocity perturbation corresponding to a 2% ξ perturbation (Fig. 8). Rayleigh

(a) **Phase velocity model**

(b) **Anisotropy model**

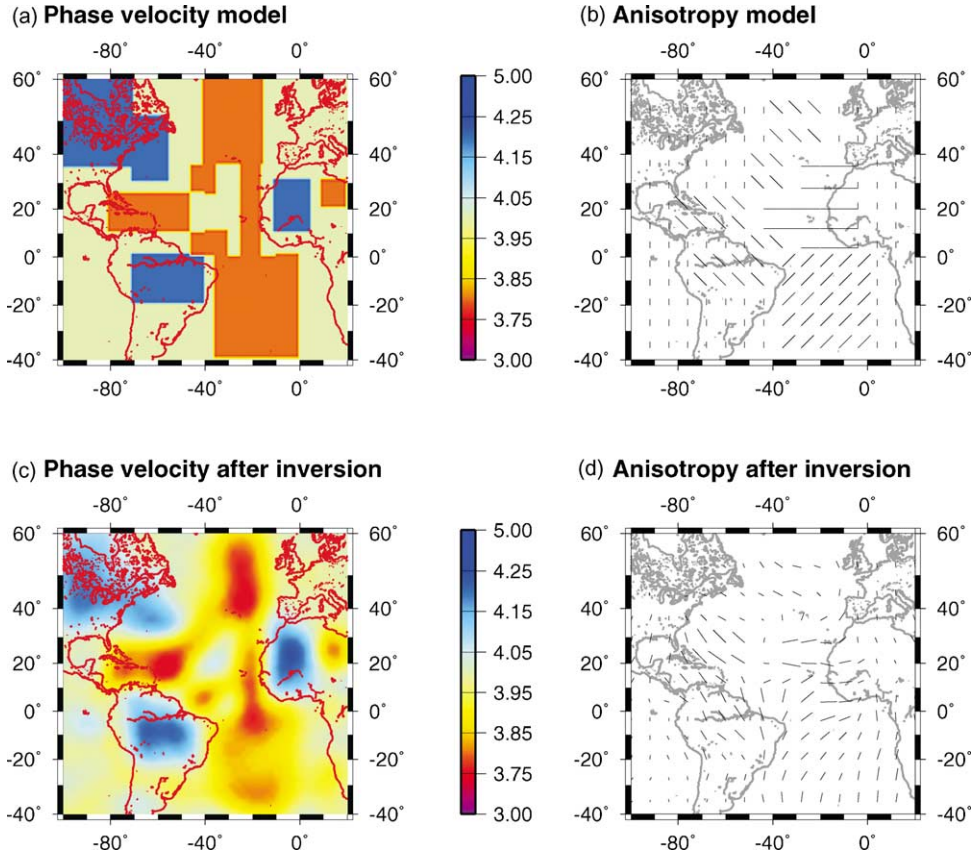(c) **Phase velocity after inversion**

(d) **Anisotropy after inversion**

Fig. 7. (a) Phase velocity model; (b) anisotropy model; (c) phase velocity after inversion; (d) anisotropy after inversion.
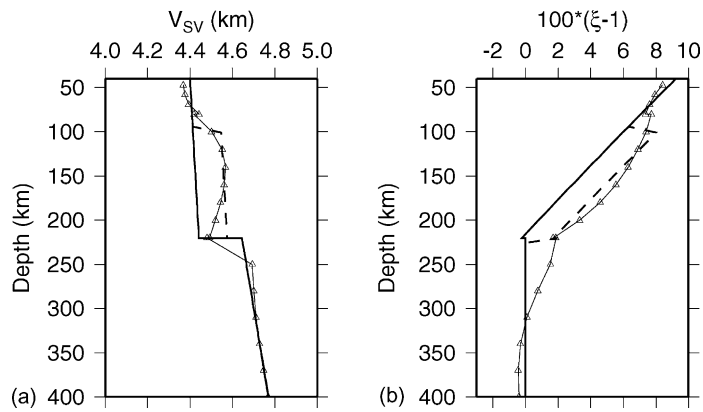
Fig. 8. Synthetic test: (a) S-wave velocity as a function of depth; (b) radial anisotropy as a function of depth. The curves correspond to the PREM model (solid line), the perturbed model that we want to retrieve (dashed line) and the inversion result (triangle).

and Love wave phase velocities are computed for this model and used as data for testing the inversion. A priori errors on data used in this synthetic test are the same that are used in the inversion of real data and they were obtained from the phase velocity regionalization presented in the paper by Silveira et al. (1998). These errors depend on period, they correspond to the resolution of the local phase velocity which is a function of the uncertainties along each path and the paths distribution. Because horizontal seismograms are noisier than vertical seismograms, the Love wave phase velocity a priori error is almost double that of Rayleigh wave phase velocities.

Fig. 8 presents the S-wave velocity and transverse isotropy for the reference model (solid line), for the model to be retrieved (dashed line) and the inversion result (triangles). Both perturbations are correctly located at depth and in amplitude, but their amplitude slightly extends beyound the layer two edges because we use a Gaussian covariance function to correlate neighboring depths in the inversion versus depth.

References

Anderson, D.L., 1982. Hotspots, polar wander, mesozoic convection and the geoid. Nature 85, 391–393.

Aslanian, D., 1993. Interactions entre les rpocessus intraplaques et les process us d'accrétio océanique: l'appont du géoide altimétrique. Ph.D. thesis, Université de Bretagne Occidentale, Brest.

Crough, S.T., 1983. Hotspot swells. Annu. Rev. Earth Planet. Sci. 11, 163–193.

Dziewonski, A., Anderson, D., 1981. Preliminary reference Earth model. Phys. Earth Planet. Inter. 25, 297–356.

Goodwin, A.M., 1985. Rooted precambrian ring shields: growth alignement, and oscillation. Am. J. Sci. 285, 481–531.

Grand, S.P., 1994. Mantle shear structure beneath the Americas and surrounding. J. Geophys. Res. 99, 591–621.

Gripp, A.E., Gordon, R.G., 1990. Current plate velocities relative to the hotspots incorporing the NUVEL-1 global plate motion model. Geophys. Res. Lett. 17, 1109–1112.

Hoffman, P.F., 1989. Speculations on Laurentia's first gigayear (2.0 to 1.0 Ga). Geology 17, 135–138.

Honda, S., Tanimoto, T., 1987. Regional 3D heterogeneities by waveform inversion-application to the Atlantic area. Geophys. J. R. Astron. Soc. 94, 737–757.

Kuo, B.Y., Forsyth, D.W., Wysession, M., 1987. Lateral heterogeneity and azimutal anisotropy in the north Atlantic determined from SS–S differential travel times. J. Geophys. Res. 92, 6421–6436.

Lévêque, J.J., Debayle, E., Maupin, V., 1989. Anisotropy in the Indian Ocean upper mantle from Rayleigh- and Love-waveform inversion. Geophys. J. Int. 133, 529–540.

Li, X.D., Romanowicz, B., 1996. Global shear-velocity model developed using nonlinear asymptotic coupling theory. J. Geophys. Res. 101, (22) 245-22,272.

McNutt, M.K., 1998. Superswells. Rev. Geophys. 36, 211–244.

Mégnin, C., Romanowicz, B., 2000. The shear velocity structure of the mantle from the inversion of body, surface and higher modes waveforms. Geophys. J. Int. 143, 709–728.

Melson, W.G., O'Hearn, T., 1986. 'Zero-age' variations in the composition of abyssal volcanic rocks. The Geology of North America. Vol M., The Western North Atlantic region, The Geological Society of America, 117–136.

Mocquet, A., Romanowicz, B., 1990. Three-dimensional structure of the upper mantle beneath the Atlantic Ocean inferred from long-period Rayleigh waves. Part II. Inversion. J. Geophys. Res. 95, 6787–6798.

Montagner, J.P., 1986. Regional three-dimensional structures using long period surface waves. Ann. Geophys. 4 (B), 283–294.

Montagner, J.P., Nataf, H.C., 1986. A simple method for inverting the azimuthal anisotropy of surface waves. J. Geophys. Res. 91, 511–520.

Nataf, H.C., Richard, Y., 1996. 3SMAC: on a priori tomographic model of the upper mantle based on geophysical modeling. Phys. Earth Planet. Inter. 95, 101–122.

Ritsema, J., van Heijst, H.J., Woodhouse, J.H., 1999. Complex shear wave velocity structure imaged beneath Africa and Iceland. Science 286, 1925–1928.

Shilling, J.G., Hanan, B.B., McCully, B., Kingsley, R.H., 1994. Influence the Sierra Leone mantle plume on the equatorial Mid-Atlantic Ridge: a Nd-Sr-Pb isotopic study. J. Geophys. Res. 99, 12005–12025.

Silveira, G., Stutzmann, E., Griot, D., Montagner, J.P., Mendes, V.L., 1998. Anisotropic tomography of the Atlantic Ocean from Rayleigh surface waves. Phys. Earth Planet. Inter. 106, 257–273.

Smith, M.L., Dahlen, F.A., 1973. The azimuthal dependence on Love and Rayleigh wave propagation in a slightly anisotropic medium. J. Geophys. Res. 78, 3321–3333.

Stutzmann, E., Montagner, J.P., 1994. Tomography of the transition zone from the inversion of higher mode surface waves. Phys. Earth Planet. Inter. 86, 99–115.

Tarantola, A., Valette, B., 1982. Generalized nonlinear inverse problems solved using least squares criterion. Rev. Geophys. Space Phys. 20, 219–232.

Windley, B.F., 1984. The Evolving Continents. Wiley, New York.

Wolfe, C., Silver, P.G., 1998. Seismic anisotropy of oceanic upper mantle: shear wave splitting methodologies and observations. J. Geophys. Res. 103, 749–771.